JOURNAL OF GEOPHYSICAL RESEARCH, VOL. 104, NO. A5, PAGES 10,285–10,294, MAY 1, 1999

Thermal plasmaspheric morphology: Effect of geomagnetic and solar activity

M. A. Reynolds,[1,2] G. Ganguli,[1] J. A. Fedder,[3,4] J. Lemaire,[5] R. R. Meier,[6] and D. J. Meléndez-Alvira[6]

Abstract. A multispecies kinetic model of the thermal plasma in the plasmasphere is used to predict the spatial dependence of the hydrogen ion and helium ion density and temperature for different levels of geomagnetic and solar activity. The particular convection electric field model chosen is intended for the time intervals between substorms. The plasma density and temperature in the equatorial plane are found to exhibit a local-time variation that is sensitive to the details of the convection electric field. In particular, the parallel temperature increases with altitude and the perpendicular temperature decreases with altitude, except in the postmidnight sector, features that are only possible if kinetic effects are taken into account. In addition, the ratio of the helium ion density to the hydrogen ion density is found to agree with observations of the Dynamics Explorer 1 satellite. This behavior can be explained by the effects of convection on the thermal particles that are magnetically trapped on closed field lines. These results have implications for the interpretation and analysis of sunlight scattered by helium ions (He II) to be measured by future global imaging satellites.

1. Introduction

Recently, there has been a resurgence of interest in the study of the plasmasphere and the plasmapause. This interest is especially topical because the upcoming IMAGE [*Burch*, 1996] and ARGOS [*McCoy et al.*, 1995] satellites will provide information on the helium ion density in the inner magnetosphere. Helium ions will be used as a surrogate for total plasma density; it is therefore important to develop a physics-based model that will predict the helium-to-hydrogen ion density ratio. Previously, observations from both geosynchronous satellites [*McComas et al.*, 1993] and polar satellites [*Horwitz et al.*, 1986] have shown a complicated dynamic behavior [e.g., *Moldwin et al.*, 1995], and the role that geomagnetic activity plays in the formation and maintenence of the plasmapause continues to be a subject of considerable interest [*Carpenter et al.*, 1993; *Ober et al.*, 1997]. Future global imaging missions will not only be able to detect the plasmapause but will also be able to infer the density variation of the plasma within the plasmasphere, such as radial profiles and asymmetries in local time. The interpretation and analysis of such images require a reliable model for the thermal plasma density morphology. Satellites, of course, have made in situ measurements of the plasmasphere, but these do not reveal the global structure, nor do they shed light on issues of causality over global scales. In addition, communications and navigation satellite systems need information on the plasmaspheric contribution to the total electron content, which can affect their operations, primarily on the nightside where the ionospheric plasma density is low. With these motivations, this paper focuses on the morphology of the plasmasphere itself.

We have developed a multispecies kinetic plasmasphere model (MSKPM) that takes into account the effect of diurnal convection on thermal plasma [*Reynolds et al.*, 1997]. A kinetic model is essential to properly include the disparate physics of the trapped particles and those in the loss cone. In the present paper, we generalize this model by including a more realistic empirical convection electric field [*McIlwain*, 1986] that depends on the magnetic activity index ***Kp***, incorporates radial shielding, and has the expected day-night asymmetry. This electric field is applicable to the time intervals between substorms. In contrast to our earlier definition [*Reynolds et al.*, 1997] of the plasmapause as the outermost closed equipotential [*Nishida*, 1966; *Brice*, 1967], we now define the plasmapause from a consideration of convective instability [*Lemaire*, 1974; 1975]. Finally, the effect of a variable solar ultraviolet flux is simulated by varying the helium ion fraction at the ion exobase. These generalizations should significantly improve the agreement between the model and observations. We demonstrate this with a comparison to in

[1]Beam Physics Branch, Plasma Physics Division, Naval Research Laboratory, Washington, D.C.

[2]Now at the Department of Physics and Astronomy, Howard University, Washington, D.C.

[3]Sachs-Freeman Associates, Inc., Landover, Maryland.

[4]Now at the Institute for Computational Sciences and Informatics, George Mason University, Fairfax, Virginia.

[5]Institut d'Aéronomie Spatiale de Belgique, Brussels, Belgium.

[6]E. O. Hulburt Center for Space Research, Naval Research Laboratory, Washington, D.C.

Paper number 1999JA900050.
0148-0227/99/1999JA900050$09.00

situ measurements of the helium-to-hydrogen ion density ratio by the Dynamics Explorer 1 (DE 1) satellite [*Craven et al.*, 1997]. It should be noted that, in its present version, MSKPM is not intended to reproduce plasmaspheric morphology during the refilling process (for example, no possibility of shocks is included).

In section 2, the plasmasphere model, MSKPM, is briefly described, and the relevant physical issues are discussed. In section 3, the convection electric field of *McIlwain* [1986] is presented, along with the density and temperature structure predicted by MSKPM when this electric field is used to drive the convection. In addition, a comparison is made with DE 1 observations of the helium-to-hydrogen density ratio. Detailed descriptions of MSKPM and the electric field model are left to the appendices.

2. Multispecies Kinetic Plasmasphere Model

MSKPM [*Reynolds et al.*, 1997] has three key features. First, it includes multiple ion species. The density of each species is determined separately, although they are coupled through the ambipolar electric field. Second, it is kinetic. There are many classes of ion orbits on closed field lines (escaping, incoming, ballistic, and trapped; see, for example, *Lemaire* [1976a]). However, they can be divided into two distinct populations, those that are in the loss cone and those that are trapped. Thermal ions that are trapped on closed field lines are not in thermodynamic contact with the ionosphere, while those in the loss cone are in continual contact. Resolving this dichotomy requires that the two populations be treated separately; therefore a kinetic treatment is necessary. Third, the model incorporates the effects of diurnal convection. Convection results in flux-tube compression and rarefaction, both in configuration space and velocity space, with corresponding local-time asymmetries in density and temperature caused by the different dynamical evolution of particles in the two populations. The mathematical details of this model are included in Appendix A, and the remainder of this section highlights the important physical properties.

The model starts with a Maxwellian velocity distribution at the ion exobase. The ion exobase is defined as the lower boundary of the ion exosphere, above which collisional effects can be neglected. A Maxwellian is chosen for simplicity, although it is straightforward to incorporate other velocity distributions. One possibility is a generalized Lorentzian distribution [*Pierrard and Lemaire*, 1996], which results in a parallel temperature that increases with altitude. Such positive temperature gradients have been observed [*Comfort*, 1986]. Here we want to focus on the effect that convection plays in determining the temperature and its anisotropy. As the exobase distribution ascends the field line, it is transformed into a source-cone (or anti-loss-cone) distribution. The particles in this source-cone distribution are in contact with the ionosphere, which means that their characteristics (such as density and temperature) are determined by the conditions at the exobase. The trapped region of velocity space is not empty but is populated by velocity-space diffusion (due to collisions and wave-particle interactions) from the loss cone over a timescale of a few days [*Lemaire*, 1989]. This trapped population is isolated from the ionosphere and therefore is strongly affected by the diurnal dynamics. Both populations, of course, play a role in determining the ambipolar potential and the global morphology. The relative density of this trapped population is presently chosen empirically through the magnitude of the parameter η explained in Appendix A, but in the future, physical processes such as velocity-space diffusion will be used to calculate its value. (The ratio of the density of the trapped to the untrapped particles is given by η multiplied by a function of position; this function of position incorporates the effects of convection.)

As each flux tube drifts diurnally under the influence of the external magnetospheric convection and corotation electric fields, there is compression and rarefaction in configuration space. The result is an increase in density when the flux tube is close to Earth and a decrease in density when the flux tube is far from Earth. This effect can be explained by the variation of the flux tube volume and can be understood in a fluid formulation [*Khazanov et al.*, 1994]. Compression and rarefaction occur in velocity space as well. This principally affects the trapped particles and is outside the scope of a fluid formulation. There are two important consequences of this "breathing" in velocity space. First, the two regions of velocity space are not in equilibrium. Second, these velocity distributions will likely drive fluctuations whose characteristics are asymmetric in local time. While it is true that the plasmaspheric densities are high close to Earth, a condition of diffusive equilibrium probably does not exist farther from Earth owing to the effects of convection. The radial motion of a flux tube is constantly rearranging the proportion of trapped and untrapped particles.

These properties were easily seen when a simple electric field was used to drive the convection [*Reynolds et al.*, 1997]. However, the details of the convection can play an important role in determining the morphology, so for the purpose of comparison with observations, it is essential to use a more realistic electric field model. The altitude and density of the exobase can also play an important role in determining the morphology; we will address this aspect in future work. It should be emphasized that this model is only applicable to the region between the exobase and the plasmapause. Outside of this region (within the ionosphere proper and on open field lines), the physics is quite different.

3. Results

3.1. External Convection Electric Field

Any external electric field can be used as input to drive convection in the present model, with two restrictions. First, the magnetic field lines are assumed to be equipotentials. Strictly speaking, this is incorrect, but because the parallel electric potential differences due to ambipolar and polarization charge separation are typically only a few volts inside the plasmasphere, it is a reasonable approximation and simplifies the analysis considerably. With this assumption the electric potential Φ needs to be specified only in the magnetic equatorial plane. No inductive electric field is included in our current model, although transient electric fields are likely to be present during the substorm growth phase. However, time-dependent electric fields will be implemented in the fu-

ture. Second, the drift trajectories (or equipotentials of Φ) are assumed to be closed. In the collisionless limit, pitch-angle scattering is ignored; in the cold plasma approximation, when the kinetic energy of the particles is small, curvature and gradient drifts are ignored. Under these assumptions all particles in a given flux tube drift along an equipotential surface of Φ, which is equivalent to ideal MHD models of magnetospheric convection. Since the model assumes that this convection is quasi-stationary and since each trajectory is treated independently, the path of each flux tube must be closed. In reality, of course, the time dependence of the drift velocity makes it impossible to determine at any given instant whether a flux tube is on an open or closed trajectory.

The outermost closed equipotential has often been identified with the plasmapause [*Nishida,* 1966; *Brice,* 1967]. This identification is problematic when the convection pattern is variable in time, for the main reason that a flux tube does not know where the future pattern will take it. Additionally, when the centrifugal potential is included, a convective instability above a certain altitude is possible. We choose to define the plasmapause in a manner that takes these issues into consideration, as proposed by *Lemaire* [1974, 1975]. In this picture, if a flux tube is beyond the "zero-parallel-force" surface, the plasma near the apex of the flux tube is convectively unstable and will be peeled off. The zero-parallel-force surface is defined as the locus of points where the centrifugal force (determined from the $\mathbf{E} \times \mathbf{B}$ velocity) balances the other field-aligned forces (gravity and polarization electric field) at the apex of the flux tube. Therefore we define the plasmapause to be the equipotential that is tangent to the zero-parallel-force surface at its deepest penetration. Under time-dependent conditions, the plasmapause will depend on the history of the convection pattern (see *Lemaire and Gringauz* [1998] for a discussion of this aspect), but we restrict the present study to quasi-stationary conditions. Defined in this manner, the plasmapause can be determined for any electric field model [*Lemaire,* 1976b].

There are many empirical models of the convection electric field, both for high latitudes and low latitudes. The simplest is a uniform field pointing from dawn to dusk [*Kavanagh et al.,* 1968], which results in a teardrop shape for the outermost closed equipotential. This field was used in a previous exposition of the model [*Reynolds et al.,* 1997]. More realistic is that of *Volland* [1973], in which the external convection potential is shielded and where the shielding is modeled in an ad hoc manner by a power law in geocentric distance. This shielding is an important physical effect that must be included in any realistic electric field. More complicated models typically consist of many terms of a spherical harmonic expansion [e.g., *Foster et al.,* 1986; *Weimer,* 1996]. This level of complexity is not necessary for the present purpose but can be added in a straightforward manner.

We have chosen to use the empirical model deduced by *McIlwain* [1986] from particle flux observations. This model incorporates three important physical effects: an electric field that is not restricted to the dawn-dusk direction, asymmetric radial shielding of the potential, and a dependence on geomagnetic activity through the *Kp* index. One important feature of this model is that the radial component of the electric field is enhanced in the postmidnight sector. A detailed description of this electric field model is given in Appendix B. Here we simply note that there are 10 parameters used as input, which quantify the physical effects just described. Figure 1 shows the equipotential contours in the magnetic equatorial plane for $Kp = 1$ and $Kp = 5$. Figure 1 and all subsequent plates and figures use the solar magnetic

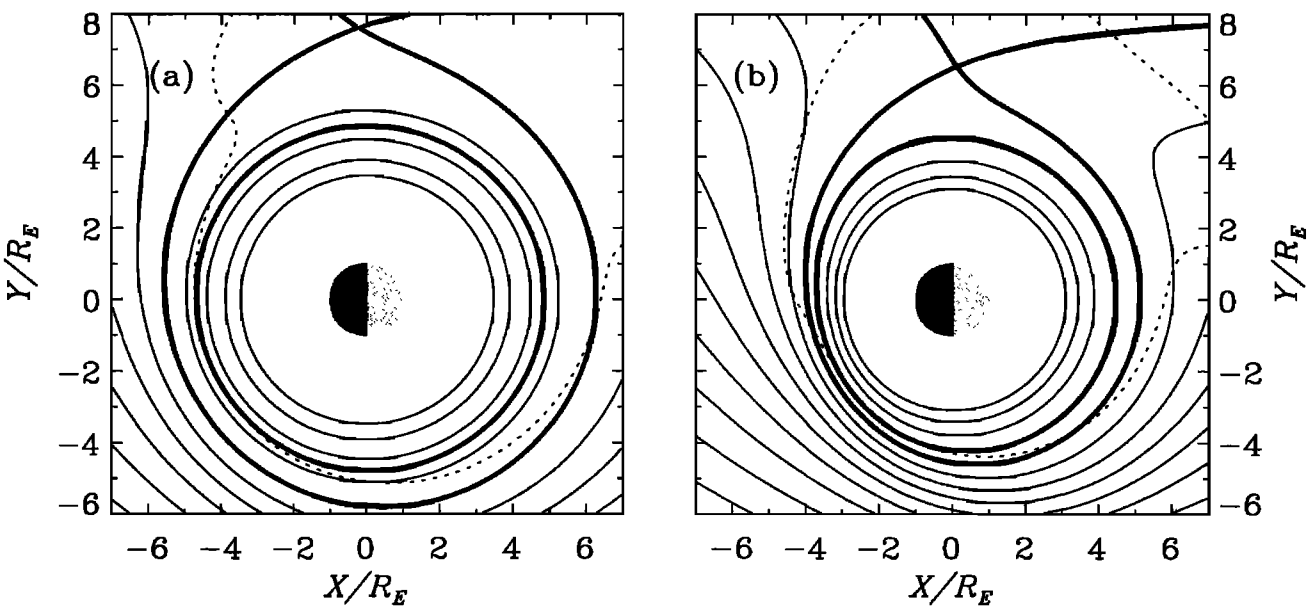

Figure 1. Equatorial equipotential contours of the convection electric field model of *McIlwain* [1986] for (a) $Kp = 1$ and (b) $Kp = 5$. The thick solid lines are the outermost closed equipotential and the plasmapause. The solid lines (thick and thin) are 3 kV apart, as measured from the outermost closed equipotential. The dotted line is the equatorial cross section of the zero-parallel-force surface. (The absolute value of the potential is arbitrary and is not indicated.) The solar magnetic (SM) coordinate system is used, with the Sun to the right.

(SM) coordinate system and view the magnetic equatorial plane from the north, with the Sun to the right. Also shown in Figure 1 are the outermost closed equipotential, the plasmapause, and the zero-parallel-force surface. For low magnetic activity the plasmapause is almost circular and is situated at approximately 5 R_E. The drift trajectories also are almost circular, so that a typical flux tube experiences little radial motion. Again, if the convection pattern is time dependent, the plasmapause will be determined by a time history consistent with the peeling process taking place in the postmidnight sector. For high magnetic activity the plasmapause is asymmetric and the flux tubes are compressed in the postmidnight sector.

The exact values of the parameters that quantitatively determine the electric field are not as important as the physical effects that are represented. For example, when $Kp = 1$, the empirical model predicts that geosynchronous orbit is outside the plasmapause. However, geosynchronous satellites observe plasmaspheric plasma at all local times when $Kp \lesssim 2$ [*McComas et al.*, 1993]. A slight change in the values of the parameters would expand the plasmapause to match these observations but would not alter the qualitative conclusions presented here. In practical terms, the parameter values that correspond to any particular state of the plasmasphere might best be determined by an inversion process using global images [*Meier et al.*, 1998].

3.2. Plasmasphere Morphology

We now discuss the effect of this external convection electric field model on the plasmasphere morphology. Because MSKPM determines the distribution functions, macroscopic quantities such as density and temperature are calculated from moments of the distribution functions in a straightforward manner.

Plate 1 shows the total plasma density in the magnetic equatorial plane as predicted by MSKPM for the electric field model shown in Figure 1. Here we have taken the exobase to be spherical and uniform, with an altitude of 3185 km ($= 0.5\ R_E$), a temperature of 3000 K, a density of 10^3 cm^{-3}, and a helium fraction of 20%. (The actual exobase is not uniform, but observations of hydrogen and helium densities show little local time variation at low latitudes.) The relative density of the trapped particles is given by the parameter $\eta = 1.75$ (see Appendix A). The convection pattern clearly determines at which local times the flux tubes are compressed and hence where the density is enhanced (compare with Figure 2 of *Reynolds et al.* [1997]). The higher density in the postmidnight sector and the corresponding lower density at other local times near the plasmapause should be detectable in global imaging experiments. The "flaring" of the density contours in Plate 1(b) near the postmidnight plasmapause is due to the asymmetry of the convection electric field. Specifically, the flux tubes reach their maximum drift velocity at an earlier local time than their closest approach to Earth, and it is between these two positions that the flaring occurs. A similar effect exists in Plate 1(a), but there it is not noticeable because the flow trajectories are almost symmetric.

Strictly speaking, the density and temperature at the exobase are simply parameters in the model. The model does not predict these values at the exobase for the following two reasons: (1) η is not unity, which formally means that the distribution is Maxwellian but not isotropic because the trapped and loss-cone populations are unequal; and (2) the discontinuity at the exobase is an artifact that means that the model does not strictly apply close to the exobase.

As noted earlier, the convection process forces a compression and rarefaction in velocity space, which results in a strong temperature anisotropy. Plates 2 and 3 show the parallel and perpendicular hydrogen temperatures in the magnetic equatorial plane for the same values of the parameters as Plate 1. (These are the true thermodynamic temperatures, obtained as moments of the distribution functions.) As expected from qualitative considerations (e.g., conservation of energy and magnetic moment), $T_\parallel > T_\perp$ when the flux tubes are far from Earth and the density is low, i.e., near the plasmapause (except postmidnight). Note that $T_\parallel$ increases with altitude for most local times. Such a positive temperature gradient has been observed routinely in the plasmasphere [*Comfort et al.*, 1985]. Previous attempts to explain these hot ions within a fluid formulation have resorted to ad hoc heating mechanisms [*Newberry et al.*, 1989; *Comfort et al.*, 1995]. Here we show that including the physics of collisionless convection results naturally in such a positive temperature gradient. Another physical mechanism that predicts positive temperature gradients and which also requires a kinetic picture is a non-Maxwellian distribution function at the exobase [*Pierrard and Lemaire*, 1996]. Including both physical effects will allow the model to agree with observations in a natural way. One consequence of the nonequilibrium nature of the distribution functions is that any fluctuations driven by microinstabilities will be asymmetric in local time. Indeed, such local-time asymmetries in the wave power spectra have been observed [*Boardsen et al.*, 1995].

3.3. Helium Ion Density

Extreme ultraviolet (EUV) images detect only the helium ion content of the plasmasphere, so it is important to understand not only the morphology of the total plasma density but also the behavior of the helium itself. Early studies [*Horwitz et al.*, 1986] concluded that the ratio of helium ion density to hydrogen ion density is relatively constant. A more recent examination of the DE 1 observations [*Craven et al.*, 1997] revealed strong statistical relationships between the helium-to-hydrogen density ratio and both geocentric distance and solar activity. On the other hand, only a weak dependence on magnetic activity and local time was observed. As will be seen next, the present model not only agrees qualitatively with these observations, but more important, they can be explained by the underlying physics.

Figure 2 shows the helium-to-hydrogen density ratio predicted by MSKPM as a function of geocentric distance r for two values of exobase helium fraction, 20% and 40%, and for two values of magnetic activity, $Kp = 1$ and $Kp = 5$. The shaded areas represent the local-time variation for $Kp = 5$, and the narrow solid areas along the bottom of the shaded areas represent the local-time variation for $Kp = 1$. For a fixed r, the spread in the density ratio is due to local-time variation. Also shown in Figure 2 is the statistical straight-line fit to the DE 1 observations deduced by *Craven et al.* [1997] for two different values of solar activity, $P = 75$ and

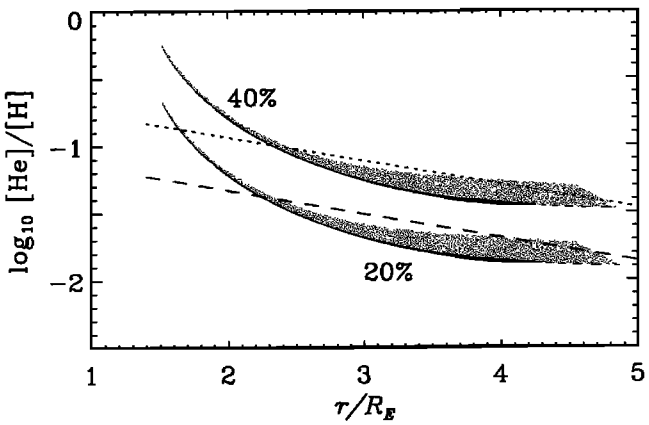

Figure 2. Ratio of the helium density to the hydrogen density as a function of geocentric distance for two values of the exobase helium fraction, 20% and 40%. The shaded areas represent the local-time variation for $Kp = 5$, and the narrow solid areas along the bottom of the shaded areas represent the local-time variation for $Kp = 1$. For comparison, the two straight lines are the statistical fit to DE 1 observations [*Craven et al.*, 1997] for two different values of the solar EUV proxy: dashed, $P = 75$; dotted, $P = 150$. The exobase is spherical and uniform, with an altitude of 3185 km ($= 0.5R_E$), a temperature of $T_0 = 3000$ K, and a density of 10^3 cm^{-3}. The relative density of the trapped particles is given by $\eta = 1.75$.

$P = 150$. (*Craven et al.* [1997] define P as a time average of the solar $F_{10.7}$ flux.)

The behavior of MSKPM is in agreement with the observations. First, there is a strong dependence on geocentric distance. This dependence is not strictly log linear, as in the statistical fit, but has a stronger variation for $r \lesssim 2R_E$. This is due simply to the fact that helium is heavier than hydrogen and is more strongly affected by the gravitational force. The stronger-than-linear variation for $r \lesssim 2R_E$ predicted by the model can be seen in the raw data of DE 1 (see Figure 3 of *Craven et al.* [1997]), but does not manifest itself in the log linear fit. (Although the DE 1 satellite was in a polar orbit and Figure 2 shows the model predictions only in the equatorial plane, a comparison between the two is valid because the model predicts similar behavior along field lines, owing to the fact that gravity acts in a spherically symmetric fashion.) Second, there is a strong dependence on solar activity. In our model, the effect of solar activity is included through a variation of the helium fraction at the exobase. This is reasonable because the production of helium ions is primarily determined by photoionization, while the density of hydrogen ions is primarily determined by charge exchange with oxygen [*Banks and Kockarts*, 1973]. Third, there is a weak dependence on local time. The physical reason for this weak dependence is that both species are affected by the convection in a similar manner. In Figure 2, for a given radial distance, there is a spread of ratios, with the largest density ratios occurring near dusk and the smallest density ratios occurring in the postmidnight sector. This local-time variation is much smaller than the variations due to geocentric distance and solar activity. Finally, there is a weak dependence on magnetic activity. That is, the difference between the solid areas and the shaded areas in Figure 2 is small compared with the radial variation. This can be understood, again, by the fact that both hydrogen and helium are affected by the convection in a similar manner.

4. Conclusion

The equatorial density and temperature morphology predicted by MSKPM exhibits a strong local-time asymmetry due to the process of large-scale convection. The increase of the parallel temperature with altitude and the structure of the temperature anisotropy are features that arise naturally from the kinetic physics.

We have focused solely on the convection process in this paper so that the results would not be masked by other effects such as a complicated exobase. A realistic exobase will have both latitudinal and longitudinal variations in altitude, density, temperature, and possibly distribution functions. These variations will affect the predictions of MSKPM and will be included for actual comparison with images.

In its present version, MSKPM can lend insight into the problem of global helium imaging. The radial dependence of the ratio of the helium density to the hydrogen density predicted by the model is in good agreement with satellite observations. This means that the values for the helium density that will be extracted from 30.4 nm images can be directly converted into total plasma density; but because convection affects both helium and hydrogen ions in a similar way, overall plasmaspheric morphology will be evident immediately from visual inspection of images. The use of an empirical model of the convection electric field will allow the retrieval of the parameters of this global field, in addition to the plasma densities, from EUV images using inversion techniques already developed [*Meier et al.*, 1998].

Appendix A: MSKPM Details

This model is applicable to the region between the exobase and the plasmapause. In the present version, this region is taken to be collisionless [*Lemaire*, 1989] and the convection of trapped particles is included. Below the exobase, Coulomb collisions dominate and the plasma distribution function is Maxwellian. Beyond the plasmapause, the trapped particles are absent because they are sporadically convected away from the corotating portion of the plasmasphere. In addition, we take the low-energy limit, ignoring both curvature and gradient drifts, and the particle motion conserves both energy and magnetic moment.

The velocity distribution is assumed to be Maxwellian at the exobase and transforms into a source-cone distribution as the particles flow up the field line. These particles will reenter the ionosphere (either in the same hemisphere or the conjugate hemisphere) in approximately 1 hour. The trapped particles in each flux tube, however, remain there indefinitely (in the limit of no diffusion) and convect under the influence of the electric field. Only those trapped particles that never encounter the exobase during their diurnal motion (and hence would be lost to the ionosphere) are included. Also, only those trapped particles that drift entirely around the Earth are

included. The distribution of the trapped particles is taken to be Maxwellian over their permitted region of velocity space, and their density, relative to that of the source cone, is determined empirically by the parameter η.

The lower boundary condition (at the exobase) on a given field line is a normalized, isotropic Maxwellian distribution f_0 for each species

$$f_0(\mathbf{v}_0) = n_0 \left(\frac{m}{2\pi k T_0}\right)^{3/2} \exp\left\{-\frac{m\left(v_{\|0}^2 + v_{\perp 0}^2\right)}{2kT_0}\right\}, \tag{A1}$$

where n_0, T_0, and $\mathbf{v}_0$ are the exobase density, temperature, and velocity, respectively, and m is the particle mass. (In general, any distribution can be used here.) The source-cone distribution f_s at a higher altitude $\mathbf{r}$ on the same field line is determined by applying Liouville's theorem (conserving energy and magnetic moment) and taking into account the accessibility condition. The result is

$$\begin{aligned} f_s(\mathbf{v},\mathbf{r}) &= f_0\left(\mathbf{v}_0(\mathbf{v})\right) \\ &\quad \times \Theta\left(\frac{B}{B_0 - B}\left[v_{\|}^2 + 2\frac{U - U_0}{m}\right] - v_{\perp}^2\right), \end{aligned} \tag{A2}$$

where Θ is the unit step function; B and U are the magnetic field and the potential energy at $\mathbf{r}$; B_0 and U_0 are those quantities at the exobase; and $\mathbf{v}_0(\mathbf{v})$ is the velocity transformation between the exobase and position $\mathbf{r}$

$$v_{\|0}^2 = v_{\|}^2 + v_{\perp}^2\left(1 - B_0/B\right) + 2(U - U_0)/m, \tag{A3a}$$

$$v_{\perp 0}^2 = v_{\perp}^2 B_0/B. \tag{A3b}$$

The potential energy U of a particle with mass m and charge q consists of the gravitational, electrostatic, and centrifugal potential energies

$$U = -\frac{GM_E m}{r} + q\phi - \frac{m}{2}\Omega^2 r^2 \cos^2\lambda, \tag{A4}$$

where M_E is the mass of the Earth, ϕ is the field-aligned electrostatic (ambipolar) potential, $\Omega \equiv E/BLR_E$ is the angular frequency of the flux tube's rotation, L is the dimensionless McIlwain parameter, R_E is the radius of the Earth, and λ is the latitude. In calculating Ω, the electric field model described in Appendix B is used, along with a dipole magnetic field. The equatorial magnetic field model of *McIlwain* [1986] is more realistic, but inside the plasmasphere ($L \lesssim 4$) it does not differ significantly from a dipole. For reasons of simplicity and convenience, therefore, we use a dipole magnetic field in the present version of MSKPM. The Θ function in (A2) indicates the region of velocity space that the source-cone distribution occupies. This region of velocity space is commonly called the loss cone. To determine the trapped distribution, we include the effects of convection on the region of velocity space left undetermined by (A2). We assume that the distribution in this region is proportional to f_0, but that accessibility limits the trapped distribution f_t to

$$\begin{aligned} f_t(\mathbf{v},\mathbf{r}) &= \eta\, f_0\left(\mathbf{v}_0(\mathbf{v})\right) \\ &\quad \times \Theta\left(v_{\perp}^2 - \frac{B}{B_{0d} - B}\left[v_{\|}^2 + 2\frac{U - U_{0d}}{m}\right]\right) \\ &\quad \times \Theta\left(\frac{B}{B_d - B}\left[v_{\|}^2 + 2\frac{U - U_d}{m}\right] - v_{\perp}^2\right), \end{aligned} \tag{A5}$$

where η is a parameter that characterizes the density of the trapped population relative to the source cone; B_d and U_d are the magnetic field and potential energy at the equator of the flux tube when the potential energy is a minimum; and B_{0d} and U_{0d} are the same quantities at the exobase of the flux tube at this same position. The local time of this "minimum potential energy" depends on the electric field model: for a uniform dawn-dusk electric field it is dawn; for the electric field given by *McIlwain* [1986] it is in the postmidnight sector. Those parameters with a subscript d are controlled by the electric field model, which determines the drift path of the flux tube, and those parameters with a subscript 0 are controlled by the field-aligned potential energy. The first Θ function in (A5) allows only those particles that do not encounter the exobase during their diurnal convection. That is, we keep only those trapped particles whose turning point is always above the exobase. The rest are assumed lost to the ionosphere when they come in contact with the exobase. The second Θ function in (A5) is the accessibility condition from the flux tube's closest approach. That is, we keep only those particles that actually drift completely around the Earth. This neglects the high-energy portion of the distribution function, but these particles have a low number density. It is important to note that η is not the density of the trapped particles relative to the density of the untrapped particles; rather, it is a weight given to the trapped distribution function. The actual density of the trapped particles is given in (A7). The value of the parameter η will depend on flux-tube filling and loss processes, as well as the recent history of the plasmasphere.

The number density is determined by integrating the distribution function over velocity space. For the source-cone population

$$\begin{aligned} n_s(\mathbf{r}) &\equiv \int d^3v f_s \\ &= n_0\left[\exp(-\psi) - A_0^{1/2}\exp\left(-\psi/A_0\right)\right], \end{aligned} \tag{A6}$$

where $\psi = (U - U_0)/kT_0$ is the dimensionless potential energy and $A_0 = 1 - B/B_0$. The density of the trapped population is

$$\begin{aligned} n_t(\mathbf{r}) &\equiv \int d^3v f_t \\ &= \eta n_0\left[A_{0d}^{1/2}\exp\left(-\psi_{0d}/A_{0d}\right)\right. \\ &\qquad \left. - A_d^{1/2}\exp\left(-\psi_{0d} - \psi_d/\beta_d\right)\right], \end{aligned} \tag{A7}$$

where $\psi_{0d} = (U - U_{0d})/kT_0$, $\psi_d = (U - U_d)/kT_0$, $A_{0d} = 1 - B/B_{0d}$, $A_d = 1 - B/B_d$, and $\beta_d = A_d/(1 - A_d)$. The total density is the sum of the two populations, $n = n_s + n_t$, as given by (A6) and (A7). In these expressions the field-aligned electrostatic potential ϕ is unknown and must be

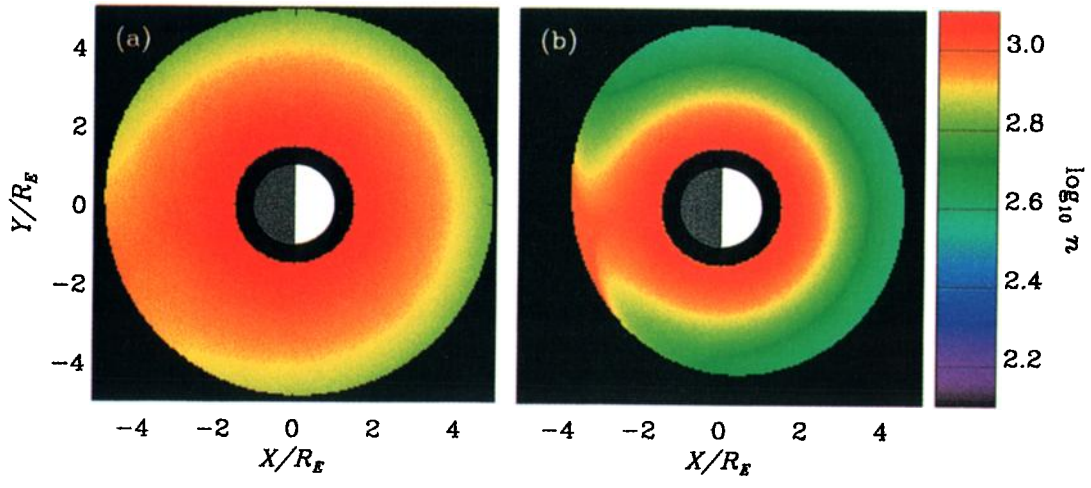

Plate 1. Plasma density n in the magnetic equatorial plane for (a) $Kp = 1$ and (b) $Kp = 5$. The exobase is spherical and uniform, with an altitude of 3185 km ($= 0.5R_E$), a temperature of $T_0 = 3000$ K, a density of 10^3 cm^{-3}, and a helium fraction of 20%. The relative density of the trapped particles is given by $\eta = 1.75$.

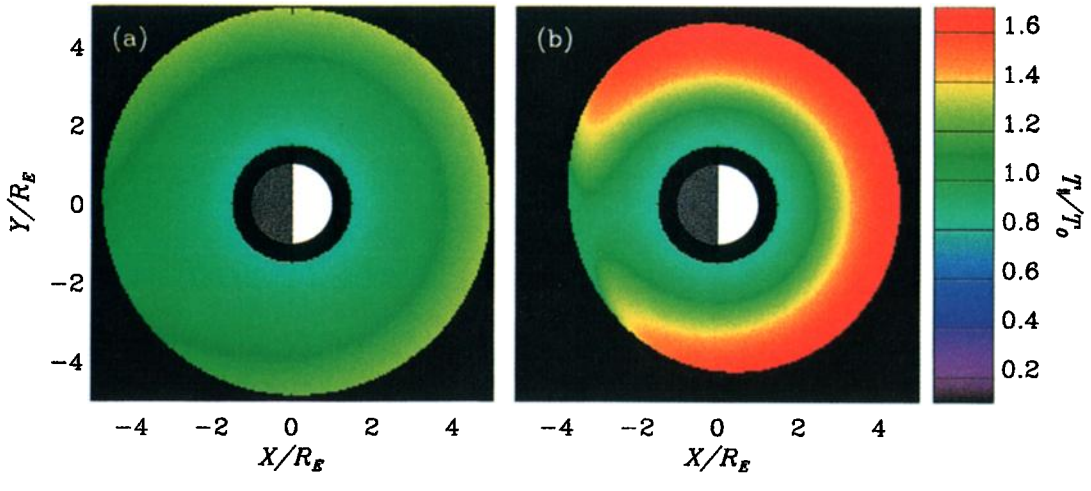

Plate 2. Parallel temperature scaled to the exobase temperature, $T\parallel/T_0$, in the magnetic equatorial plane for (a) $Kp = 1$ and (b) $Kp = 5$. The exobase is spherical and uniform, with an altitude of 3185 km ($= 0.5R_E$), a temperature of $T_0 = 3000$ K, a density of 10^3 cm^{-3}, and a helium fraction of 20%. The relative density of the trapped particles is given by $\eta = 1.75$.

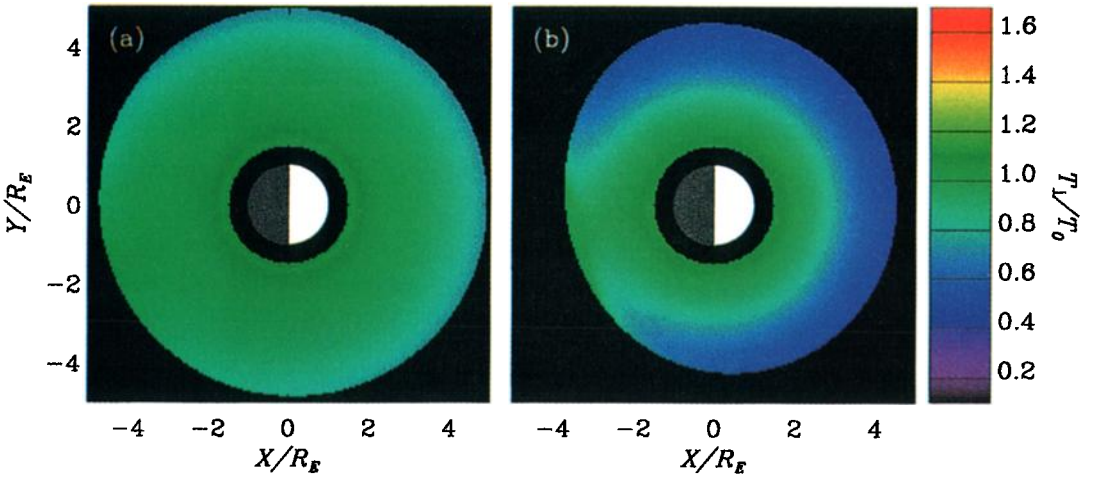

Plate 3. Perpendicular temperature scaled to the exobase temperature, $T\perp/T_0$, in the magnetic equatorial plane for (a) $Kp = 1$ and (b) $Kp = 5$. The exobase is spherical and uniform, with an altitude of 3185 km ($= 0.5R_E$), a temperature of $T_0 = 3000$ K, a density of 10^3 cm^{-3}, and a helium fraction of 20%. The relative density of the trapped particles is given by $\eta = 1.75$.

calculated self-consistently by applying the quasineutrality condition $n_e = \sum_i n_i$. The electrons are treated in the same manner as the ions, with $T_e = T_i$.

Besides the density, knowledge of the total distribution allows the calculation of the thermodynamic temperature, determined from the second-order moment of the velocity distribution function. This integral gives the diagonal elements of the pressure tensor (for the choice of a Maxwellian distribution at the exobase, the off-diagonal elements are zero). In the parallel direction,

$$P_{\parallel_s} \equiv \int d^3v \left(mv_\parallel^2\right) f_s \tag{A8}$$
$$= n_0 T_0 \left[\exp(-\psi) - A_0^{3/2} \exp\left(-\psi/A_0\right)\right],$$

$$P_{\parallel_t} \equiv \int d^3v \left(mv_\parallel^2\right) f_t \tag{A9}$$
$$= \eta n_0 T_0 \left[A_{0d}^{3/2} \exp\left(-\psi_{0d}/A_{0d}\right) - A_d^{3/2} \exp\left(-\psi_{0d} - \psi_d/\beta_d\right)\right].$$

The thermodynamic temperature in the parallel direction is obtained from the total pressure weighted by the total density

$$T_\parallel = \frac{P_{\parallel_s} + P_{\parallel_t}}{n_s + n_t}. \tag{A10}$$

The perpendicular components of the pressure tensor are

$$P_{\perp s} \equiv \frac{1}{2}\int d^3v \left(mv_\perp^2\right) f_s \tag{A11}$$
$$= n_0 T_0 \left[\exp(-\psi) - \exp\left(-\psi/A_0\right)\left\{A_0^{1/2}\left(1 + \frac{\psi}{\beta_0}\right) + \frac{A_0^{3/2}}{2\beta_0}\right\}\right],$$

$$P_{\perp t} \equiv \frac{1}{2}\int d^3v \left(mv_\perp^2\right) f_t = \tag{A12}$$
$$\eta n_0 T_0 \left[\exp\left(-\psi_{0d}/A_{0d}\right)\left\{A_{0d}^{1/2}\left(1 + \frac{\psi_{0d}}{\beta_{0d}}\right) + \frac{A_{0d}^{3/2}}{2\beta_{0d}}\right\} - \exp\left(-\psi_{0d} - \psi_d/\beta_d\right)\left\{A_d^{1/2}\left(1 + \frac{\psi_d}{\beta_d}\right) + \frac{A_d^{3/2}}{2\beta_d}\right\}\right],$$

where $\beta_0 = A_0/(1 - A_0)$ and $\beta_{0d} = A_{0d}/(1 - A_{0d})$. The factors of 1/2 appear because the perpendicular direction has 2 degrees of freedom. The perpendicular thermodynamic temperature is obtained in the same manner as the parallel temperature

$$T_\perp = \frac{P_{\perp s} + P_{\perp t}}{n_s + n_t}. \tag{A13}$$

More complicated distributions functions can be used for f_0 (e.g., drifting Maxwellian or generalized Lorentzian distributions) and other velocity moments of the distribution can be calculated (e.g., flows and heat flux).

The expressions for the source-cone population, (A6), (A8), and (A11), are equivalent to those given by *Lemaire* [1976a] for the ballistic and escaping particles at position A. The expressions for the trapped population, (A7), (A9), and (A12), are similar to those given by *Lemaire* [1976a] for the regions t_1 and t_2 at position A, but with the effects of convection included in the accessibility condition. Because we have defined the subscript d to refer to the position of minimum potential energy as the flux tube convects around the Earth, we do not encounter a situation like position B of *Lemaire* [1976a].

Appendix B: Electric Field Model

McIlwain [1986] has developed a useful empirical model of the equatorial convection electric field. Like that of *Brice* [1967], it consists of two contributions, a corotation potential Φ_{co} and an external convection potential Φ_{ext}. In this appendix, we describe this model in detail, paying special attention to the relevant physics.

The total potential, $\Phi = \Phi_{co} + \Phi_{ext}$, is expressed as a function of the two spatial coordinates in the equatorial plane, geocentric distance r and azimuthal angle φ, the magnetic activity index Kp, and 10 parameters. (Here we use the SM coordinate system in the magnetic equatorial plane, and φ is measured eastward from noon.) The corotation potential, which does not include the effect of the dipole tilt, is

$$\Phi_{co} = -9.2 \times 10^4 \text{ V} \frac{R_E}{r}. \tag{B1}$$

The external convection potential consists of a uniform electric field of arbitrary direction (i.e., not necessarily in the dawn-dusk direction) shielded asymmetrically by the auroral ring and enhanced by magnetic activity. This external convection potential has the form

$$\Phi_{ext} = \Phi_{uni}\, \mathcal{E}(Kp)\, \mathcal{S}, \tag{B2}$$

where Φ_{uni} is the potential of a uniform electric field with components E_x and E_y, offset an amount Φ_{off} from the corotation potential,

$$\Phi_{uni} = -r\left(E_x \cos\varphi + E_y \sin\varphi\right) + \Phi_{off}, \tag{B3}$$

$\mathcal{E}$ is an enhancement factor that increases monotonically with Kp,

$$\mathcal{E} = 1 + \alpha K_r, \tag{B4}$$

$K_r = Kp/(1 + 0.1Kp)$ is a modified Kp index, and $\mathcal{S}$ represents the radial shielding factor,

$$\mathcal{S} = \frac{1}{1 + \left(r_0/r\right)^\gamma}, \tag{B5}$$

whose shielding radius r_0 has a value of

$$r_0 = \beta R_E \left\{S_1 - S_2 \cos\varphi + K_r\left(S_3 - S_4 \cos\varphi\right)\right\}. \tag{B6}$$

The shielding radius r_0 is proportional to the radius of the auroral ring.

The 10 parameters are S_1, S_2, S_3, S_4, α, β, E_x, E_y, Φ_{off}, and γ. Of course, β is not independent, but it does carry

physical meaning in that it allows the shielding transition to occur equatorward of the auroral ring. The specific realization used in this paper is given by the following set of values (see *McIlwain* [1986] for details): $S_1 = 9.8$, $S_2 = -1.4$, $S_3 = -0.9$, $S_4 = -0.3$, $\alpha = 0.3$, $\beta = 0.8$, $E_x = 0.03$ mV/m, $E_y = 0.12$ mV/m, $\Phi_{\text{off}} = 3.0$ kV, and $\gamma = 8$. In this realization, the uniform electric field is not purely in the dawn-dusk direction but is rotated 13° from dusk toward the Sun.

The shielding behavior is quite important. The specific functional form given in (B5) exhibits the realistic behavior of $S \to 1$ for $r \to \infty$ and $S \to 0$ for $r \to 0$. There is a transition at $r = r_0$, with a transition width Δr given by

$$\frac{\Delta r}{r_0} = \frac{2}{\gamma}. \tag{B7}$$

This implies that for large γ the transition is very sharp. For the values used here, $r_0/R_E \approx 8 - Kp$ and $\Delta r \approx 2R_E$, with slight dependences on local time.

For the purpose of inverting global images in order to obtain values of a parametrized model, the electric field as it stands is not suitable. There are redundant parameters and the dependence on Kp does not necessarily have the correct form. For image inversion, a simplified version, yet one with all the essential physics, would be

$$\Phi = -\frac{\Phi_1}{r} - \frac{r(\Phi_2 \cos\varphi + \Phi_3 \sin\varphi) + \Phi_4}{1 + \{(\Phi_5 - \Phi_6 \cos\varphi)/r\}^{\Phi_7}}, \tag{B8}$$

where $(\Phi_1, \ldots, \Phi_7)$ are the seven essential parameters. Of course, to determine the density, other parameters will enter, namely, the exobase density, temperature, and helium fraction, bringing the total of parameters to 10. The robustness of this model to the inversion process has yet to be determined.

Acknowledgments. This work is sponsored by the Office of Naval Research and the National Aeronautics and Space Administration. M. A. R. thanks the National Research Council for support as an NRC-NRL Research Associate.

Janet G. Luhmann thanks Richard H. Comfort and G. Khazanov for their assistance in evaluating this paper.

References

Banks, P. M., and G. Kockarts, *Aeronomy, Part B,* 355 pp., Academic, **San Diego, Calif., 1973.**

Boardsen, S. A., J. L. Green, S. F. Fung, and W. W. L. Taylor, Plasma wave imaging of the Earth's magnetosphere, *Eos Trans. AGU, 76*(46), Fall Meet. Suppl., F521, 1995.

Brice, N. M., Bulk motion of the magnetosphere, *J. Geophys. Res., 72,* 5193-5211, 1967.

Burch, J. L., IMAGE Overview, *Eos Trans. AGU, 77*(46), Fall Meet. Suppl., F564, 1996.

Carpenter, D. L., B. L. Giles, C. R. Chappell, P. M. E. Decreau, R. R. Anderson, A. M. Persoon, A. J. Smith, Y. Corcuff, and P. Canu, Plasmasphere dynamics in the duskside bulge region: A new look at an old topic, *J. Geophys. Res., 98,* 19243-19271, 1993.

Comfort, R. H., Plasmasphere thermal structure as measured by ISEE-1 and DE-1, *Adv. Space Res., 6*(3), 31-40, 1986.

Comfort, R. H., J. H. Waite Jr., and C. R. Chappell, Thermal ion temperatures from the retarding ion mass spectrometer on DE 1, *J. Geophys. Res., 90,* 3475-3486, 1985.

Comfort, R. H., P. G. Richards, P. D. Craven, and M. O. Chandler, Problems in simulating ion temperatures in low density flux tubes, in *Cross-Scale Coupling in Space Plasmas, Geophys. Monogr. Ser.,* vol. 93, edited by J. L. Horwitz, N. Singh, and J. L. Burch, pp. 155-160, AGU, Washington, D.C., 1995.

Craven, P. D., D. L. Gallagher, and R. H. Comfort, Relative concentration of He^+ in the inner magnetosphere as observed by the DE 1 retarding ion mass spectrometer, *J. Geophys. Res., 102,* 2279-2289, 1997.

Foster, J. C., J. M. Holt, R. G. Musgrave, and D. S. Evans, Ionospheric convection associated with discrete levels of particle precipitation, *Geophys. Res. Lett., 13,* 656-659, 1986.

Horwitz, J. L., L. H. Brace, R. H. Comfort, and C. R. Chappell, Dual-spacecraft measurements of plasmasphere-ionosphere coupling, *J. Geophys. Res., 91,* 11203-11216, 1986.

Kavanagh, L. D., Jr., J. W. Freeman Jr., and A. J. Chen, Plasma flow in the magnetosphere, *J. Geophys. Res., 73,* 5511-5519, 1968.

Khazanov, G. V., C. E. Rasmussen, Yu. V. Konikov, T. I. Gombosi, and A. F. Nagy, Effect of magnetospheric convection on thermal plasma in the inner magnetosphere, *J. Geophys. Res., 99,* 5923-5934, 1994.

Lemaire, J., The 'Roche-limit' of ionospheric plasma and the formation of the plasmapause, *Planet. Space Sci., 22,* 757-766, 1974.

Lemaire, J., The mechanisms of formation of the plasmapause, *Ann. Geophys., 31,* 175-189, 1975.

Lemaire, J., Rotating ion-exospheres, *Planet. Space Sci., 24,* 975-985, 1976a.

Lemaire, J., Steady state plasmapause positions deduced from McIlwain's electric field models, *J. Atmos. Terr. Phys., 38,* 1041-1046, 1976b.

Lemaire, J., Plasma distribution models in a rotating magnetic dipole and refilling of plasmaspheric flux tubes, *Phys. Fluids B, 1,* 1519-1525, 1989.

Lemaire, J. F., and K. I. Gringauz, *The Earth's Plasmasphere,* 350 pp., Cambridge Univ. Press, New York, 1998.

McComas, D. J., S. J. Bame, B. L. Barraclough, J. R. Donart, R. C. Elphic, J. T. Gosling, M. B. Moldwin, K. R. Moore and M. F. Thomsen, Magnetospheric plasma analyzer: Initial three-spacecraft observations from geosynchronous orbit, *J. Geophys. Res., 98,* 13453-13465, 1993.

McCoy, R. P., K. F. Dymond, J. M. Picone, G. R. Carruthers, O. A. Kelley, and D. D. Cleary, Hyperspectral imaging of the global ionosphere from the ARGOS satellite, paper presented at the International Symposium on Spectral Sensing Research, Int. Soc. for Photogramm. and Remote Sens., Melbourne, Australia, Nov. 26 to Dec. 1, 1995.

McIlwain, C. E., A K_p dependent equatorial electric field model, *Adv. Space Res., 6*(3), 187-197, 1986.

Meier, R. R., A. C. Nicholas, J. M. Picone, D. J. Melendez-Alvira, G. I. Ganguli, M. A. Reynolds, and E. C. Roelof, Inversion of plasmaspheric EUV remote sensing data from the STP 72-1 satellite, *J. Geophys. Res., 103,* 17505-17518, 1998.

Moldwin, M. B., M. F. Thomsen, S. J. Bame, and D. McComas, The fine-scale structure of the outer plasmasphere, *J. Geophys. Res., 100,* 8021-8029, 1995.

Newberry, I. T., R. H. Comfort, P. G. Richards, and C. R. Chappell, Thermal He^+ in the plasmasphere: Comparison of observations with numerical calculations, *J. Geophys. Res., 94,* 15265-15276, 1989.

Nishida, A., Formation of plasmapause, or magnetospheric plasma knee, by the combined action of magnetospheric convection and plasma escape from the tail, *J. Geophys. Res., 71,* 5669-5679, 1966.

Ober, D. M., J. L. Horwitz, and D. L. Gallagher, Formation of density troughs embedded in the outer plasmasphere by subauroral ion drift events, *J. Geophys. Res., 102,* 14595-14602, 1997.

Pierrard, V., and J. Lemaire, Lorentzian ion exosphere model, *J. Geophys. Res., 101,* 7923-7934, 1996. (Correction, *J. Geophys. Res., 103,* 4117, 1998.)

Reynolds, M. A., G. Ganguli, J. A. Fedder, and D. J. Meléndez-Alvira, Effect of diurnal convection on trapped thermal plasma in the outer plasmasphere, *Geophys. Res. Lett., 24,* 2255-2258, 1997.

Volland, H., A semiempirical model of large-scale magnetospheric electric fields, *J. Geophys. Res., 78,* 171-180, 1973.

Weimer, D. R., A flexible, IMF dependent model of high-latitude electric potentials having "space weather" applications, *Geophys. Res. Lett., 23,* 2549-2252, 1996.

J. A. Fedder, Institute for Computational Sciences and Informatics, George Mason University, Fairfax, VA 22030.

G. Ganguli, Code 6794, Naval Research Laboratory, 4555 Overlook Avenue SW, Washington, DC 20375.

J. Lemaire, Institut d'Aéronomie Spatiale, B-1180, Bruxelles, Belgium.

R. R. Meier and D. J. Meléndez-Alvira, Code 7640, Naval Research Laboratory, 4555 Overlook Avenue SW, Washington, DC 20375.

M. A. Reynolds, Department of Physics and Astronomy, Howard University, 2355 6th Street NW, Washington, DC 20059. (email: mareynolds@physics1.howard.edu)

(Received June 22, 1998; revised December 22, 1998;
accepted January 26, 1999.)